Materials Science in Semiconductor Processing 92 (2019) 28–38

Contents lists available at ScienceDirect

Materials Science in Semiconductor Processing

journal homepage: www.elsevier.com/locate/mssp

Si:optical device materials

Electronic transitions in low dimensional semiconductor structures measured by surface photovoltage spectroscopy

Daniela Cavalcoli*, Maria Antonietta Fazio

Physics and Astronomy Dept. University of Bologna, viale C. Berti Pichat 6/II, Italy

ARTICLE INFO

Keywords:
Surface photovoltage
Optical gap
Electronic transitions
Optical applications
Nanoporous germanium
Silicon nanocrystals
InGaN/GaN heterostructures

ABSTRACT

Aim of the present contribution is to review several results obtained by the application of surface photovoltage spectroscopy method to low dimensional semiconductors. Photo-induced electronic transitions have been detected in: heterostructures based on III-nitrides, Si-based nanostructures (nanowires and nanocrystals) and nanoporous Ge layers. The effect of two-dimensional electron gas and of quantum confinement on the energy of band-to-band transitions in these structures has been studied. The results show that Surface Potovoltage Spectroscopy is a flexible and non-destructive method capable to reveal phase changes, Burstein Moss effects, doping-related features, light trapping and quantum confinement effects in low dimensional structures that can be useful for several optoelectronic applications.

1. Introduction

The development of optical devices in the last decades has led to a new paradigm: solid state lighting, i.e. a type of lighting that uses semiconductor light-emitting diodes (LEDs) as sources of illumination instead of electrical filaments or plasma. Highly efficient solid state lighting can provide large environmental benefits as it leads to a substantial reduction of electrical energy consumption. Optical devices based on semiconductor low dimensional structures are the building blocks of this technology: quantum wells, heterostructures and quantum dots are all devices where the strong overlapping between the electronic wave functions gives rise to radiative recombination and thus efficient light emission.

In the present contribution, the detection of electronic transitions in selected low dimensional semiconductors by Surface Photovoltage Spectroscopy (SPV spectroscopy or SPS) is reported.

SPS has been used since the early seventies by Gatos and Lagowski (1973) [1] to characterize semiconductor surfaces (determination of surface potential, flat band potential), oxides deposited on different surfaces (oxide thickness, oxide integrity, oxide charge, plasma damage) and bulk properties (measurements of minority carrier lifetimes and diffusion lengths, doping densities). In addition, starting from 1999 [2–4], the method has been applied to the study of surface, interface and defect states in semiconductors.

Nowadays, the method is widely used to detect electronic transitions (band-to-band, defect-band, surface states-bands) in nano- and low dimensional semiconductor systems, as in these systems SPS shows several advantages. Indeed, the method does not require cumbersome sample preparation, junction formation, etc. and it can be also applied on buried layers, deposited thin films, heterostructures, multi-phase and nano-structures, where standard transmission optical spectroscopies are not applicable.

Very recently, surface photovoltage has been used to extract information on charge generation and collection mechanisms in different materials, such as low dimensional systems important for solar energy conversion and harvesting. To cite some examples, photochemistry of a mercaptoethanol-ligated CdSe quantum dot, used in quantum dots solar cells, has been investigated by SPS [5]; charge separation across WSe_2-MoS_2 lateral heterostructures has been investigated by SPV combined with Kelvin Probe microscopy (KPM), showing promising photovoltaic applications [6]; photopotential across a $Ru-SrTiO_3$:Rh/$BiVO_4$ particle tandem, which can be used as water splitting photocatalyst, has been measured by SPS [7]; the role of the selective contacts and the Tauc gap in organic perovskites for photovoltaic applications ($CH_3NH_3PbI_3$ and $MAPbI_{3-x}Cl_x$) has been clarified using surface photovoltage spectroscopy [8,9]. All these examples show the ability of SPV spectroscopy to measure directly built-in voltages, sub-band gap states, and effective band gaps. It is a very valuable method for deepening the understanding of charge injection and collection processes in materials and nanostructures.

In addition, surface photovoltage has been used to investigate nanostructures and materials important for optoelectronic applications. For example, an efficient charge separation has been demonstrated in Ge nanocrystals by SPS [10]; local behaviour of the photogenerated

* Corresponding author.
E-mail addresses: daniela.cavalcoli@unibo.it, cavalcoli@bo.infn.it (D. Cavalcoli).

https://doi.org/10.1016/j.mssp.2018.05.027
Received 5 March 2018; Received in revised form 16 May 2018; Accepted 21 May 2018
Available online 28 May 2018
1369-8001/

carriers in silicon nanopillars has been investigated by SPV in combination with KPM [11] and efficient charge transport in silicon photoanode for water oxidation has been demonstrated by SPV [12]. Finally, SPS has always allowed for a clear understanding on the role of defects on optical properties; to cite an example, the role of yellow band on photoluminescence of AlGaN/GaN heterostructures has been clarified by SPS [13].

As the knowledge of band-to-band or defect-band electronic transitions in a certain material and/or structure is fundamental to explore the capabilities of that system as optical device, in the present contribution we will describe the detection of such electronic transitions in low dimensional structures that find or could find applications in such field.

In this review, we will describe the physical basis and the experimental set-up of the method only briefly, as the details have been deeply described elsewhere [3,4,14]; then we will focus on some examples relevant to the application of the method to materials and systems of interest for optical applications. In particular, the results on GaN based heterostructures, Si nanowires and nanocrystals, nanoporous Ge films will be presented and discussed.

2. Physical basis and experimental set-up

The Surface PhotoVoltage (SPV) is an illumination-induced change in the equilibrium surface potential V_s, which is due to charge transfer and/or redistribution within the device. The driving force for the charge transfer is the built-in electric field generated either by the surface space charge region or by the junction space charge region. The surface photovoltage is thus defined as the difference between the surface potential under illumination V_s(ill) and the surface potential in dark V_s(dark):

$$SPV = V_S(ill) - V_S(dark) \quad (1)$$

The SPV signal can be detected by illuminating the surface with above or below band gap light. To obtain a continuous spectrum of SPV *vs* the incident photon energy, a tuneable source is usually employed.

When photons with energy equal or larger than the band gap hit the semiconductor surface, electron-hole pairs are generated and collected by the surface barrier; a significant amount of charge may transfer in opposite directions under the built-in electric field and/or redistribute within the surface or the bulk. In this way, the net surface charge density changes and the surface potential is consequently reduced. The variation recorded in the SPV spectrum when the incident photon energy approaches band-to-band transitions constitutes the most significant feature in the SPV spectrum, and the optical band gap E_G can be obtained from it.

In the spectral region close to the band-gap, photons can induce free charge to transfer between shallow states extending from the band gap (also known as Urbach tails) to one of the bands. The amplitude of the *tail states* can also be evaluated from a SPV spectrum [14].

For photon energies larger than the band gap a saturation value should be reached by the SPV signal, but often strong electron-hole recombination at the surface significantly reduces the collected SPV signal. Further features that can be detected in the above band gap region of the spectrum can be related to phase segregations or Van Hove singularities [3,4]. Finally, it is worth mentioning that, as the SPV signal is proportional to the optical absorption coefficient α [3,4], SPV spectroscopy can also be used for the detection of bulk defect states.

SPV spectroscopy requires a tuneable light source to inject free carriers into the semiconductor sample, an external or internal electric field to separate carriers, a detector and an amplifier of the relevant signal. Usually, a photon source (quartz-tungsten-halogen or xenon lamp, depending on the spectral range of the experiment) coupled with a grating monochromator is used to inject carriers. Free carrier separation can be obtained by the electric field generated by a pn or Schottky junction (in contact mode) or by the surface space charge region (in non-contact mode). The detection is usually accomplished by a probe capacitively coupled with the sample and the signal is amplified through phase sensitive amplification. Further details on the experimental set up have been published elsewhere [14].

3. Results

In the present section, selected applications of the SPV spectroscopy to the study of defect and surface states in low dimensional semiconductor nanostructures are reported. In detail, interface states in III-N based heterostructures, optical band gap in Si nanocrystals and nanowires, and optical gap in nanoporous Ge are presented.

3.1. Electronic transitions in III-nitride alloys

In the last few years, III-nitride (III-N) semiconductors and their alloys have shown high potential for interesting applications in photonics and electronics. III-N based heterostructures have been under wide investigation for different applications such as ultraviolet photodetector, light emitters, etc. [15]. For example, white light emitting diodes (LEDs) based on III-nitride InGaN/GaN quantum wells currently offer the highest overall efficiency for solid state lighting applications [16].

SPV has already proved to be a useful method to investigate III-N alloys heterostructures. The role of growth technique, doping, and crystal polarity on the kinetics of photo-generated charges in GaN has been studied by time resolved SPS by Winnerl et al., and electrical properties of crystallographic defects in ternary AlGaN and quaternary Al(Ga,In)N alloys have been studied by light-assisted Kelvin probe force microscopy [17].

In this section some results on the application of SPS to the investigations of ternary (InGaN) and quaternary (AlInGaN) alloys will be reviewed. The following example shows the determination of band-to-band and below band gap transitions in good quality Si doped InGaN layers [18]. The InGaN band gap (E_G(InGaN)) varies nonlinearly as a function of In content (x), following a modified Vegard's law:

$$E_G(In_xGa_{1-x}N) = (1-x)E_G(GaN) + xE_G(InN) - bx(1-x) \quad (2)$$

with $E_G(GaN)$ and $E_G(InN)$ GaN and InN energy gaps, respectively, and b bowing parameter accounting for non-linear effects. Up to now, no agreement has been reached on the bowing parameter value and even on the issue if a single one could describe the gap over its entire composition range [19,20].

Fig. 1a shows SPV spectra of the InGaN/GaN samples for different In content (In%). $In_xGa_{1-x}N$/GaN heterostructures grown by Metal Organic Chemical Vapour Deposition (MOCVD) by AIXTRON have been analysed. The sample structure is sketched in its inset. The nominal barrier layer thickness of InGaN is 40–45 nm for all samples, while the buffer layer (GaN) is 4 μm thick. Two main peaks are evident in all the SPV spectra. The first one at 3.4 eV, is related to band-to-band transitions in the GaN substrate; the second one, at varying energies between 2.4 and 2.8 eV, is linked to the band-to-band transitions in the InGaN top layer. The variation of this value for each sample is correlated to the In content within the layer. Therefore, it is evident the SPV spectroscopy power to determine the band gap of both top (InGaN) and buried layers (GaN). By this measurement, the energy gap of the InGaN alloys as a function of In content could be extracted and plotted in Fig. 1b, compared with literature results [19,21,22] and fitted with Eq. (2) to extract the bowing parameter, whose value results in good agreement with literature data [18].

At energies below band gap, SPV spectroscopy is usually employed to determine defect or impurity states. Among several possible dopants introduced in InGaN layers, silicon is particularly appealing since its presence mitigates the effect of the polarization field which acts as a barrier for the charge carriers, being detrimental in InGaN based solar cells as it strongly reduces the carrier collection efficiency. In addition,

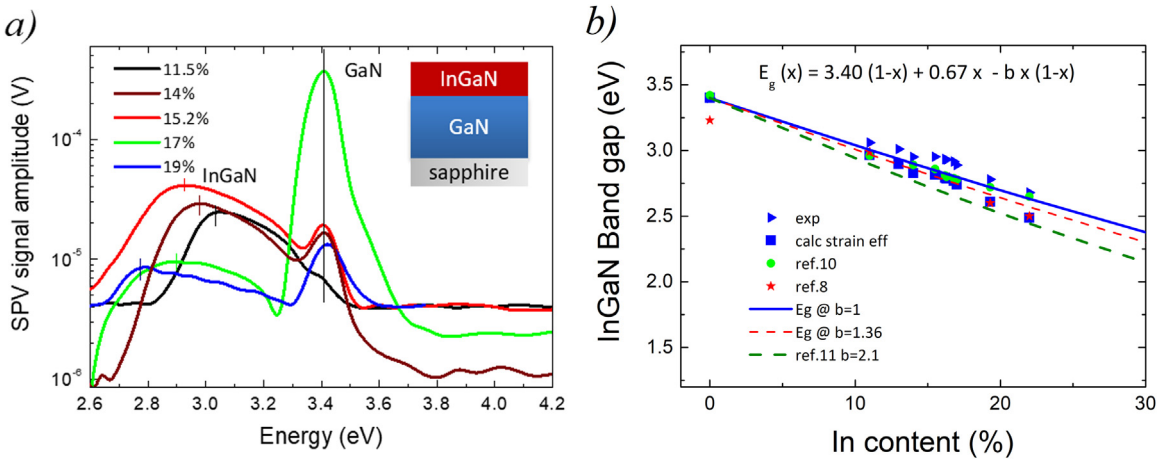

Fig. 1. a) SPV spectra of InGaN/GaN structures with different In content; the sketch of the structure appears in the inset. b) Experimental values of the optical energy gap of $In_xGa_{1-x}N$ layers (In content up to 22%, blue solid triangles) and results with added strain effect (blue solid squares), compared with earlier reported results (green solid circles, red solid stars) in references [19,21,22]. The lines show the calculated trend for different bowing parameters in the linear region (up to 20% In). *Reprinted from* [17]. (For interpretation of the references to color in this figure legend, the reader is referred to the web version of this article.).

Si doping helps reducing the dislocation lines in InGaN/GaN heterostructures [23,24].

Fig. 2a shows SPV spectra of Si-doped InGaN/GaN heterostructures with different In contents. For samples 19% and 22% In (red and blue curves, respectively), positive slope variations in the photon energy range below InGaN band gap can be noted in the spectra. Since Si doping leads to an n-type conductivity, the positive slope changes can be related to electronic transitions from the valence band to the Si shallow donor levels close to the conduction band. These levels appear at Ev + 2.74, Ev + 2.64, Ev + 2.50 eV for In% 14, 19, 22, respectively. A comparison in the SPV spectra between undoped and doped structures with comparable In% could be extracted and the results are plotted in Fig. 2b. It can be observed that Si doping is responsible for both an enhancement of the SPV signal and the appearance of the slope changes in the below InGaN band gap region. Therefore, these transitions can be related to Si donor levels, and thus the activation energy of Si in InGaN for different In% can be extracted. The results are plotted in Fig. 2c as black squares. By this analysis it can be established that Si related energy levels become shallower as the In% increases. As a consequence, the ionized donor concentration grows, as reported in Fig. 2c (red dots), leading to an increased efficiency of Si doping in InGaN. The enhancement of the doping efficiency can be related to substitution of In by Si within the layers [18].

Another interesting example of the application of SPV spectroscopy to III-Ns based alloys concerns nearly lattice matched $Al_{1-x}In_xN$/AlN/GaN heterostructures. These structures have been recently widely studied due to promising applications in the area of solid state lighting. Due to the potential barrier well forming at the interface between $Al_{1-x}In_xN$ and GaN, these heterostructures exhibit typical 2D electron gas (2DEG) confined at the heterointerface with a density of the order of $1.0–2.0 \times 10^{13}$ cm^{-2}. The addition of an AlN layer has a double role: it better helps the confinement of electrons and facilitates the reduction of alloy scattering. It has been demonstrated that the 2DEG density varies as a function of the AlN layer thickness *d*; in particular, it increases for a range of *d* between 0 and 2.5 nm [25,26].

In Fig. 3a a sketch of the investigated AlInN/AlN/GaN structures is depicted. The samples have been grown by MOCVD by AIXTRON as well [26,27]. The investigated samples structures are the same and only differ in the AlN layer thickness. Their SPV spectra are reported in Fig. 3b. As already explained in the previous section, the most relevant peak in a SPV spectrum is usually related to band-to-band electronic transitions. Furthermore, the change in the photon energy causes a variation of the optical absorption coefficient α and thus of the penetration depth α^{-1}. Considering the spectral variation of α^{-1} in AlInN, AlN and GaN [27], it can be guaranteed that for photon energies around 3 eV the carriers generation and collection mainly occur within the GaN layer. Whereas, at larger photon energies, comparable to the GaN band gap, these processes occur mainly at the interface between GaN and AlN, or at the GaN surface in the template sample. Thus, the peaks in the spectra are all related to band-to band transitions at the AlN/GaN interface (Fig. 3b) or at the GaN surface (reported in Fig. 3c). In the GaN template the peak maximum in the spectra expectedly occurs at 3.44 eV (Fig. 3c), in good agreement with the optical gap E_G in GaN reported in literature [28], while in the heterostructures the corresponding features are detected at higher energy values (Fig. 3b). This shift in the band gap depends on the AlN interlayer thickness *d*. It could not be revealed by optical transmission measurements, as shown in Fig. 3d, since no difference in the optical transmittance spectra between GaN template and the 1 nm AlN heterostructures has been evidenced.

Since the energy gap shift is present only in the heterostructures, it can be linked to the presence of the 2DEG, whose density changes with the AlN layer thickness. In proximity of the hetero-interface, the semiconductor becomes almost degenerate. In addition, the energy gap increases as a function of the free carriers concentration, linked to the 2DEG density due to the combined Moss Burstein and renormalization effects, as sketched in Fig. 4a. The energy gap shift ΔE_G obtained by SPV spectroscopy monotonically increases as a function of the free carrier concentration n_e, as reported in Fig. 4b (red squares for the experimental data and red solid curve for the fit). The comparison between experimental data and theoretical predictions allows for the evaluation of the effective mass dependence on free carrier concentration, reported in the black dashed line in Fig. 4b, by means of a parameter which quantitatively accounts for the non-parabolic conduction band [27]. It is worth noting that in this application SPV allows for the local determination of band-to-band transitions i.e. the energy gap is measured at the interface, where the effect of the 2DEG is significant. The same analyses would be impossible by optical transmission spectroscopy, which is not able to detect the shift. This bandgap shift has to be taken into account in all applications where this material is used to emit light via radiative band-to-band recombination.

3.2. *Electronic transitions in Si nanostructures*

Surface photovoltage spectroscopy has also shown unique potentialities in the case of nanosized semiconductor structures, whose properties have been reviewed by [29].

Among Si nanostructures, Si nanowires show increasing interest and promising applications in several fields, such as photovoltaics, due to

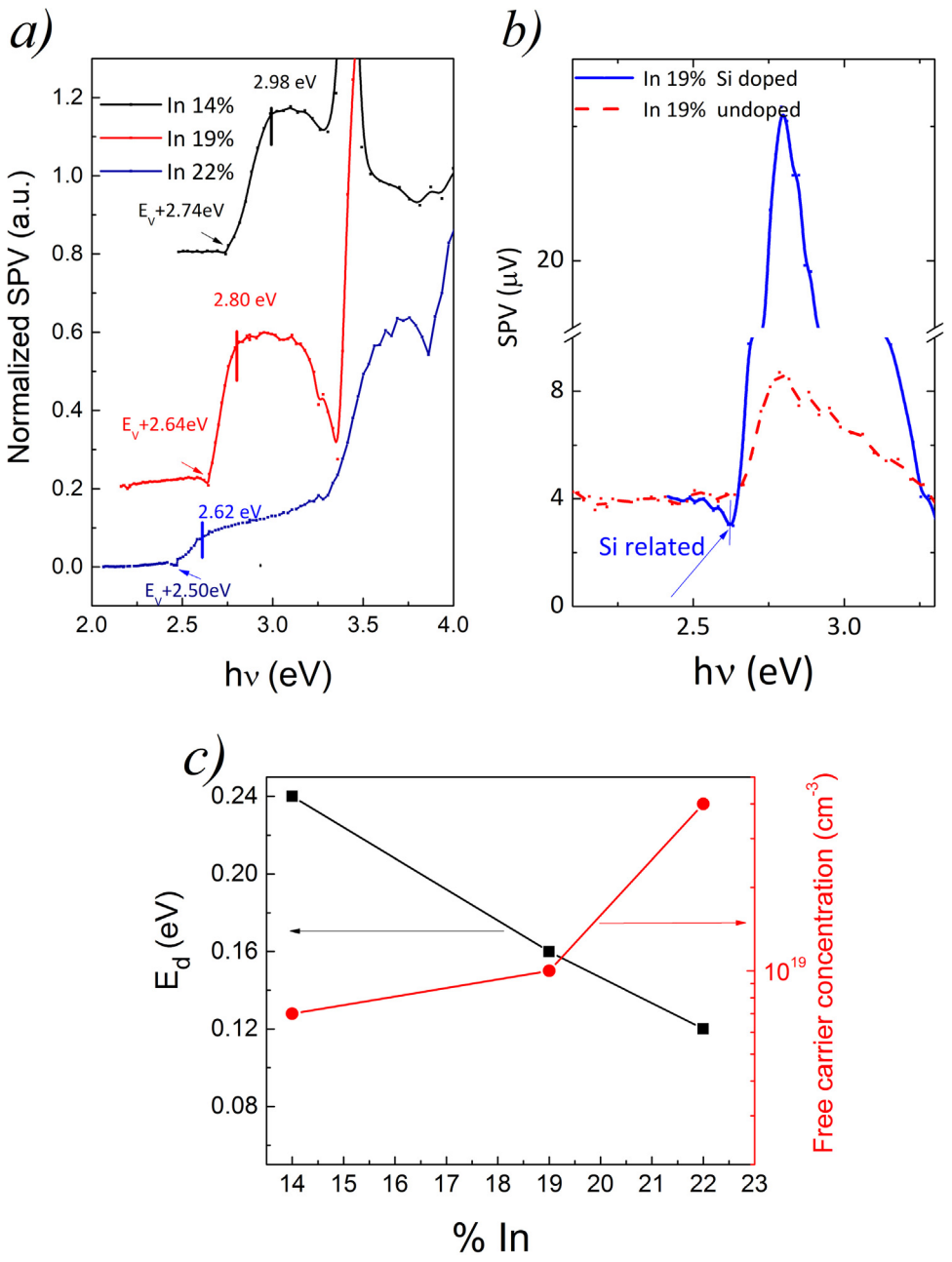

Fig. 2. a) Normalized SPV spectra of the Si doped InGaN samples with 14%, 19% and 22% In content. The spectra have been shifted for clarity. Energy gap values and below band gap transitions are marked in the graph. b) SPV spectra of undoped InGaN structure compared to a Si doped one (same In content, 19%). c) Variation of Si related donor levels (black squares) vs In% (left axis). The results are measured by SPV and calculated from the conduction band edge of InGaN. The variation of free carrier concentration vs In% (solid circle) is also shown (right axis). The data have been measured by electrochemical capacitance voltage analyses. *Reprinted from* [18]. (For interpretation of the references to color in this figure, the reader is referred to the web version of this article.).

diameter-tunable optical absorption and optical bandgap [30], and optoelectronics and photochemistry, in the case of optically active porous structures [31].

Band-to-band transitions have been measured by SPV spectroscopy in Si nanowires (NWs) [32]. Gold catalysed silicon NWs have been grown on Si substrate at a total pressure ranging from 8 to 10 Torr using a cold wall Chemical Vapour Deposition (CVD) chamber. N-type and p-type doping has been obtained using B_2H_6 and PH_3 gases during deposition, respectively, in order to include B and P atoms within the layers. A scanning electron micrograph of the Si NW mat is visible in the inset of Fig. 5. Further details on NWs properties are reported by [32]. In Fig. 5 the SPV spectra of undoped, B and P doped Si NWs are compared to that of bulk Si. As already outlined in previous sections, changing the photon energy causes the optical absorption coefficient α and in turn the penetration depth α^{-1} variation. For photon energies in the range from 0.8 to 1.4 eV, the penetration depth in bulk Si ranges from 10^6 to 10 μm [33]. Thus, in this spectral range the carriers are generated and then collected mainly within the Si substrate. Whereas, these processes mainly occur within the NW mat when photon energies are above 1.4 eV. It is clear from the comparison shown in Fig. 5 that all the samples show an onset at around 1 eV, i.e. the energy gap of Si. Moreover, B doped and undoped NWs show an additional feature at c.a. 1.6 eV. Since at these photon energies the carrier generation and collection are channelled within the NW mats, this feature can be safely related to the NWs. Due to Urbach tails presence induced by crystal disorder within the structure, smooth optical transitions occur. This broadening does not allow for a more precise determination of the optical band gap, which must be associated to a low error bar around 0.1 eV. Therefore, it can be concluded that the optical gap of B doped and undoped NWs is equal to 1.6 eV, while the P doped one is 1.0 eV. This huge difference can be explained by a phase transition induced by doping in Si NWs. The great majority of undoped NWs shows totally wurtzite phase; structural and optical measurements show that B doped NWs mats predominantly keep this structure, while P doped ones mainly change it into a diamond phase [32]. In this example, it has been shown how SPV spectroscopy allows for determining phase

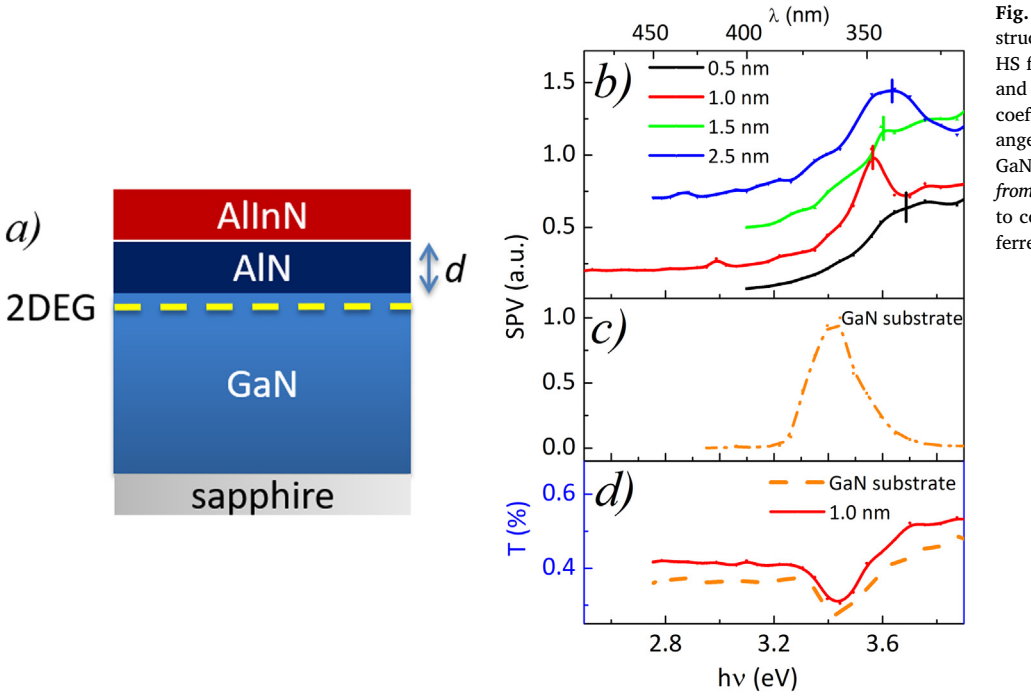

Fig. 3. a) Sketch of AlInN/ AlN/GaN heterostructure (HS) and b) SPV (a.u.) spectra of the HS for different thicknesses d of the AlN layer and c) of the GaN template. d) Transmission coefficient (T) spectra of GaN template (orange, dashed line) and of AlInN/AlN(1 nm)/GaN heterostructure (red, solid line). *Reprinted from* [27]. (For interpretation of the references to color in this figure legend, the reader is referred to the web version of this article.).

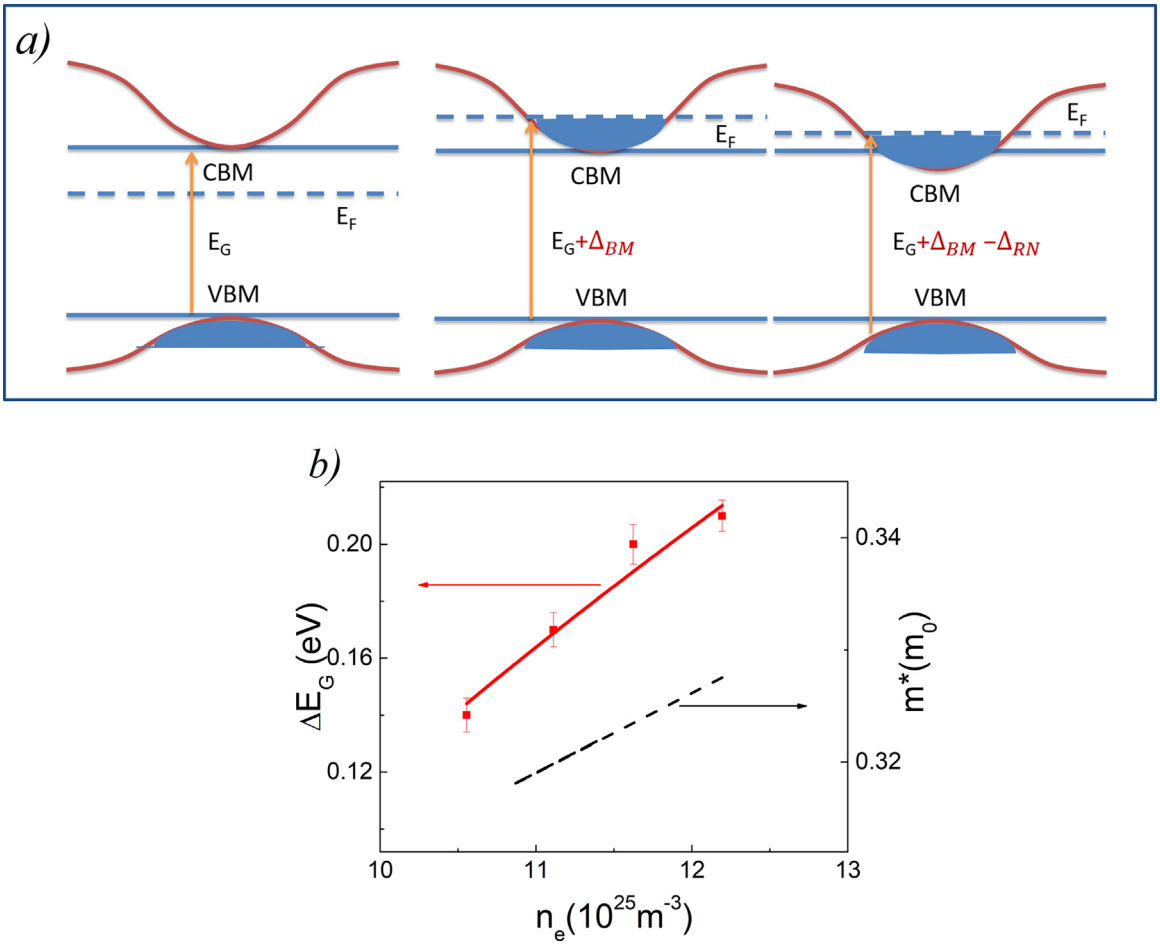

Fig. 4. a) Sketch of the Moss Burstein (center) and additional renormalization effects (right) and b) experimental values (red squares) and fitted curve (red solid line) of the band gap shift ΔE_G as a function of free carrier concentration n_e. Calculated values of the electron effective mass m^* are plotted as a function of free carrier concentration n_e (black dashed line). *Fig. 4b is reprinted from* [27]. (For interpretation of the references to color in this figure legend, the reader is referred to the web version of this article.).

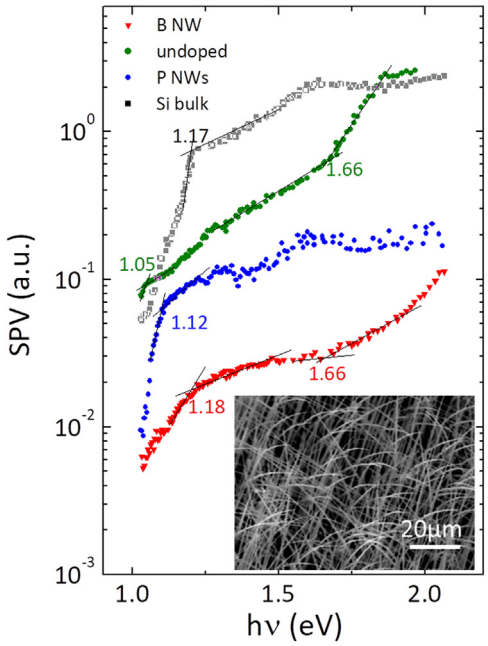

Fig. 5. SPV spectra of bulk Si (black squares) and undoped (big green dots), P doped (little blue dots) and B doped (red triangles) Si NWs. The slope changes occur at the estimated optical band gaps, for B doped and undoped Si NWs (1.6 ± 0.1) eV, for P doped NWs and bulk Si (1.1 ± 0.1) eV. The scanning electron micrograph of the NW mat is shown in the inset. *Reprinted from* [32]. (For interpretation of the references to color in this figure legend, the reader is referred to the web version of this article.).

changes in Si based nanowires.

Another interesting Si based nanostructure is made by Si nanocrystals (NCs) embedded in different matrices. Quantum confinement effects can be achieved in these structures when the dimensions of the Si nanocrystals are smaller or of the order of the Bohr radius in the equivalent mass approximation, and in addition the embedding matrix is made by a semiconductor with a larger energy gap than Si. These effects lead to the tunability of the band gap and to the suppression of non-radiative recombination paths; these materials properties have been explored in view of several interesting applications, ranging from optical devices, solar cells, and radiation detectors [29]. Therefore, the characterization of electronic transitions in these structures is necessary to explore their possible applications.

In the present section, the study of electronic transitions at Si nanocrystals embedded in different matrices by surface photovoltage spectroscopy method will be presented.

The first example is related to hydrogenated nanocrystalline Si (nc-Si:H). nc-Si:H is a multiphase material consisting of an amorphous Si matrix and dispersed Si nanocrystals (NCs). The films have been deposited on crystalline Si by Low Energy Plasma Enhanced Chemical Vapour Deposition (LEPECVD) with different dilution rates. The measured crystalline fractions of the obtained samples range between 20% and 80%. An SPV spectrum for a sample with high crystallinity (75%) and low hydrogen dilution (3%) is reported as an example in Fig. 6a. The knee that occurs in the spectrum at 1.59 eV corresponds to the energy gap (E_G) of the film. This energy value is typical of the films with high crystallinity. In this case, the dimension of the Si nanocrystals range from 5 to 15 nm [34], little enough to cause free carriers localization at Si NCs. Therefore, the spectrum below bandgap could be fitted with the sum of three Lorentzian functions plus an exponential function whose factor determine the Urbach tail and thus the crystal disorder of the a-Si matrix. The Lorentzian peaks are linked to the transitions assisted by localized states, at 1.31, 1.41 and 1.51 eV, while Urbach tails in the present samples are of about 80 meV. Fig. 6b shows a sketch of the proposed band diagram of the material. It can be noted that the analyses of spectra have allowed for the detection of electronic transitions between localized states, which could be ascribed to quantum confinement effects at Si NCs. Quantum confinement occurs when the interface between amorphous and crystalline phases acts as potential energy barrier for moving electrons. However, as stated in Section 2, SPV requires not only carrier generation but also carrier collection. Thus, charge carriers must be separated by the surface junction electric field and must flow within the film to be detected by SPV. For this reason, electronic transitions at fully localized states could not be, in principle, detected by SPV. Therefore, we must conclude that free carriers at Si NCs are only partially localized, according to theoretical prediction from [35]. Free carriers generated at the Si nanocrystals may be collected as they can thermally exit the potential barrier. They can both tunnel out of the quantum dot or be separated by the surface electric field. In conclusion, SPV spectroscopy has allowed for the identification of electronic transitions at partially localized states at Si NCs.

Another example of quantum confinement effect at Si NCs revealed by SPV spectroscopy is shown in the following section. Nanocrystalline silicon oxynitride (nc-SiO_xN_y) layers have been deposited by Plasma Enhanced Chemical Vapour Deposition (PECVD) on Float Zone silicon. These materials can be used as emitter layers in Si heterojunction solar cells [36], as passivated contacts for photovoltaic applications [37], or as optical fibres [38]. The incorporation of oxygen and nitrogen into the amorphous matrix widens the optical bandgap (up to 2.2 eV), with a consequent reduction of parasitic absorption within the material.

Among the precursor gases, nitrous oxide (N_2O) was introduced to include more or less oxygen and nitrogen within the layers [37]. Then, in order to obtain NCs formation, some layers have been annealed at 800 °C in nitrogen atmosphere [37]. Fig. 6c shows SPV spectra of three nc-SiO_xN_y samples obtained by varying O content and by adding or not an annealing step after deposition (L0h, low oxygen content, as-deposited; L3h, low oxygen content, annealed for 3 h; H3h, high oxygen content, annealed for 3 h) as black lines. As demonstrated by structural measurements, low/high oxygen content results in low/high crystal disorder, while the annealing step promotes crystallization within the layers. Further information on the sample processing and characterization are reported in ref [37]. As main features in a SPV spectrum are related to slope changes, the derivative of the signal dSPV/dE shows peaks that can be directly related to the electronic transitions. The derivatives of the spectra are reported in Fig. 6c as red lines. First of all, a general decrease of the SPV signal with increasing energy can be observed for all the samples (Fig. 6c), related to a decrease of the light penetration depth with increasing photon energy. In particular, this effect is more pronounced for H3h sample and it might be due to wider Urbach tails, related to an enhanced degree of crystal disorder. This result is in agreement with previous studies [37]: the incorporation of more oxygen within the amorphous network followed by an annealing step leads to oxygen relocation, higher disorder and lower crystalline fraction. On the contrary, the sample L3h, which is the one with the highest crystal fraction, shows features in the spectrum even at higher photon energies that can be better evidenced in its derivative (red curve in Fig. 6c, central position). Due to the drop towards zero in L0h and H3h spectra, the derivative spectra have been considered up to almost 2.2 eV, since above this value the SPV signal almost vanishes and thus the derivative becomes useless.

A maximum can be clearly distinguished in the derivative spectra of the three samples at lower photon energies, which might indicate the energy position of the bandgaps of the layers, ranging from 1.75 to 1.90 eV. These values have a trend in agreement with the Tauc gaps trend extracted from absorption measurements [37]. The derivative spectra of all the samples show a series of features (minima and maxima). This finding might be an indication of quantum confinement effects occurring at the Si NCs, which are formed within the amorphous matrix due to the annealing treatment, as reported in [37]. The

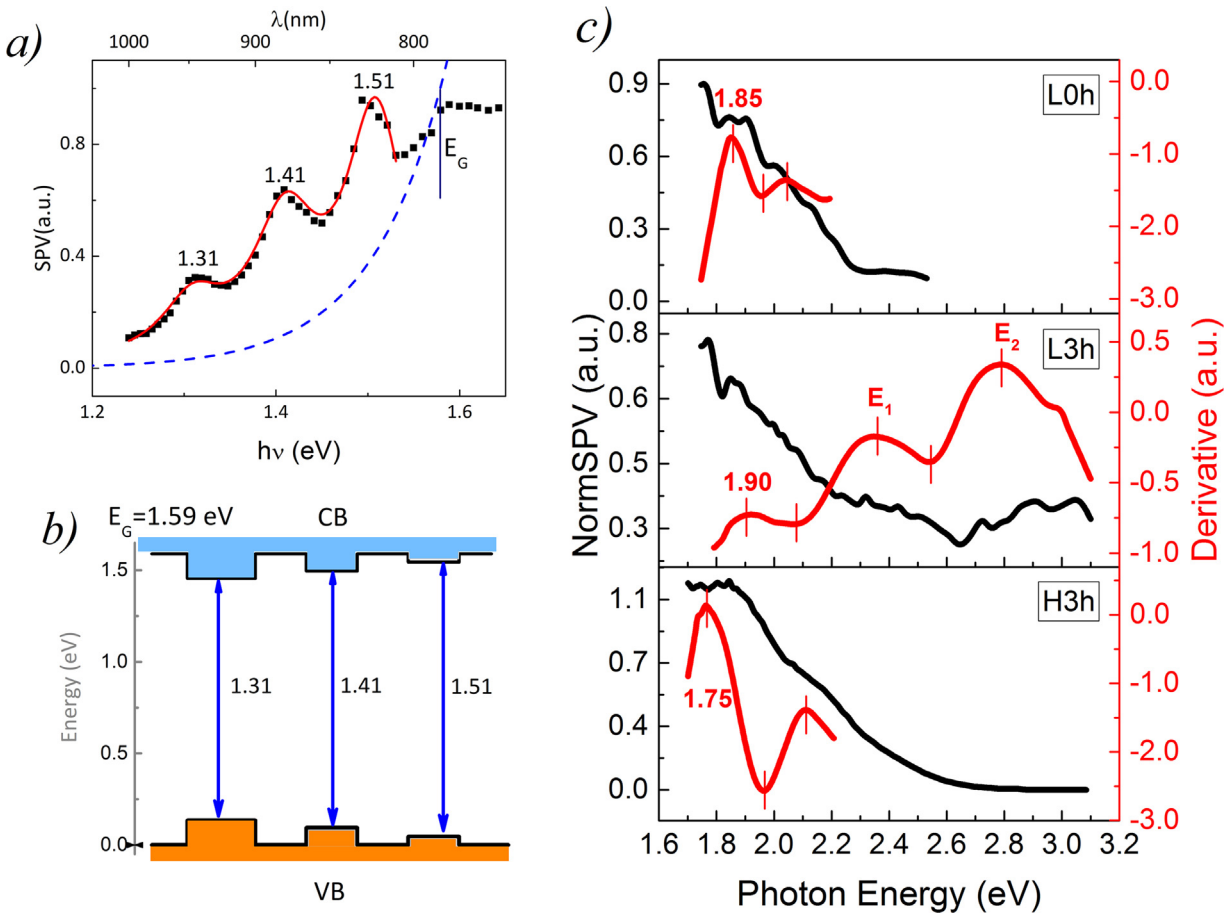

Fig. 6. a) Experimental SPV spectrum (dark squares) of nc-Si:H film highly crystalline (75%), grown at low hydrogen dilution (3%). The fitting function is the sum of three Lorentz functions (centered at 1.31, 1.41 and 1.51 eV) (solid line) plus an Urbach tail contribution due to the amorphous matrix (dashed line). The Lorenzian peaks have been related to electronic transitions at partially localized states. b) Sketch of the band diagram resulting from the SPV spectrum of Fig. 6a. *Reprinted from* [34]. c) Normalized SPV (black line) and corresponding derivative spectra (red line), obtained using the Xenon lamp, for the three samples: L0h (low O content, as-deposited), top; L3h (low O content, 3 h annealed), center; and H3h (high O content, 3 h annealed) bottom. (For interpretation of the references to color in this figure legend, the reader is referred to the web version of this article.).

absorption spectra of 0D confined structures typically consist of a series of discrete peaks at energies higher than the bulk bandgap, corresponding to optical transitions between different electron and hole levels, as shown in Fig. 6b [39]. In particular, the derivative spectrum of L3h layer shows a higher signal with respect to the other samples and reveals the presence of additional features at energies higher than the bandgap. Some of the features in the L3h derivative spectrum (E_1 = (2.33 ± 0.05) eV and E_2 = (2.78 ± 0.05) eV) appear to be in agreement with the results from single-dot spectroscopy studies on silicon quantum dots in an amorphous oxide matrix, reported by Sychugov et al. [40]. The appearance of above band-gap features in the L0h and H3h derivative spectra could also be related to quantum confinement at Si nanocrystals, even if they are present in these samples in smaller density [37].

3.3. Electronic transitions in porous semiconductors

As already mentioned in Section 1, the study of photoinduced electronic transitions by SPV spectroscopy is possible without the need of a Schottky or pn junction, as often required by junction spectroscopy methods, like for example Deep Level Transient Spectroscopy (DLTS) technique. This advantage is powerful, and it becomes essential to investigate materials containing pores or voids. In this case, the presence of very rough surfaces makes the realization of a Schottky junction challenging. In this perspective, porous semiconductors depict an incisive example to reveal SPV spectroscopy potentiality. Moreover, this method also allows to investigate electronic transitions in layers grown on non-transparent substrates, as generally occurs in the case of porous thin films. In the last few years, great interest has been focused on semiconductor materials containing nanopores, due to their large surface-to-volume ratio and their enhanced capability to adsorb foreign species (atoms, ions and molecules), thus promoting their employment in several appealing and innovative applications. Emerging applications of porous semiconductors embrace a variety of innovative sensors, solar cells and optical devices [41]. SPV studies of porous Si, TiO_2 and Ge have been reported recently [42–45]. Moreover, porous semiconductors can also be efficiently decorated with metallic nanoparticles, an appealing subject in recent years in a plethora of applications such as Surface-Enhanced Raman Scattering (SERS) [46] and bio sensors [47]. In the present example, surface photovoltage studies of ion implanted nanoporous Ge samples will be discussed [44].

Nanoporous Ge (np-Ge) samples both in bulk and thin film structures have been studied in [44,45]. The thin film arrangement is remarkably appealing in low cost applications, since they are cheaper and more flexible than bulk solutions [48,49]. Bulk np-Ge samples have been obtained by ion implantation (1×10^{16} cm^{-2}, 300 keV Ge^+ at room temperature) of Sb doped (n-type) Ge Czochralski (100) crystals. A porous amorphous layer lies on a continuous amorphous layer, on top of crystalline bulk Ge. After ion implantation, a selection of samples has been annealed at temperatures ranging from 360 to 500 °C for 1 h, in order to promote crystallization. On the other hand, 200-nm-thick thin film np-Ge samples have been obtained by MBE on SiO_2 film (500 nm

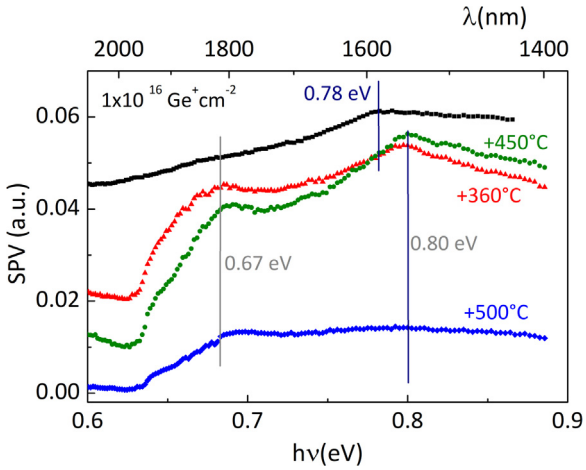

Fig. 7. Normalized SPV spectra of nanoporous Ge layers with the same implant fluence at different annealing temperatures. The spectra have been shifted for sake of clarity. The feature at 0.78 eV is related to the main electronic transition in the amorphous phase, while the ones at 0.67 and 0.80 eV correspond to the main transitions in the crystalline phase. Ge fluence (Ge^+/cm^{-2}) and annealing temperatures (°C) are shown in the plot. The curves are shifted along the y axis for sake of clarity. *Reprinted from* [43].

thick) thermally grown on Si substrates. To achieve a polycrystalline structure, the substrate temperature during depositions was kept at 400 °C [50]. The samples have been then implanted with different Ge^+ fluences (1×10^{16} and 2×10^{16} Ge^+/cm^{-2}) at 300 keV to produce porous amorphous films. Some implanted samples have been annealed in a conventional furnace at 500 °C for 1 h, in N_2 atmosphere.

The first investigation on the bulk np-Ge samples concerns the evolution of the noticeable features in the SPV spectra with the change in the annealing temperature. The SPV spectra of bulk np-Ge samples are presented in Fig. 7: an as-implanted nanoporous sample (black squares) is compared to those obtained with the same implant fluence (1×10^{16} cm^{-2}) but annealed at increasing temperature values. The SPV spectrum of the as-implanted sample reveals one main feature at 0.78 eV, which is a typical value for band-to-band transitions in the amorphous phase; while, in the presence of a thermal step, two different features gradually appear as the annealing temperature increases, at 0.67 and 0.80 eV, respectively. These slope changes can be related to band-to-band transitions in crystalline Ge [33 and ref. therein]. These results are in good agreement with the micrograph analyses [49], which confirm that a thermal step at these annealing temperatures causes crystallization within the samples. The broadening of the spectra in Fig. 7 is likely due to large tail state formation, a proof of the presence of crystal disorder within the layers.

Beyond bare np-Ge samples, several nanoporous Ge samples decorated with Au nanoparticles (NP) have been studied by SPV method. A selection of np-Ge samples was decorated with Au NP by electrochemical deposition at a fixed potential but different deposition times, and their SPV spectra have been studied. The implant fluence of 1×10^{16} cm^{-2} has been kept constant. Fig. 8a–c show the cross section Transmission Electron Microscopy (X-TEM) images of the np-Ge samples decorated with Au nanoparticles for 10, 20 and 40 s deposition time, respectively. In addition, Fig. 8d depicts the relevant SPV spectra of these samples compared to a non-decorated reference sample; they represent the raw data of the measurements, which are not normalized to the photon flux spectrum. With respect to the reference sample, a remarkable increase of the SPV signal occurs for Au deposition time of 20 s in Fig. 8d, while a decrease is evident for 10 and 40 s deposition

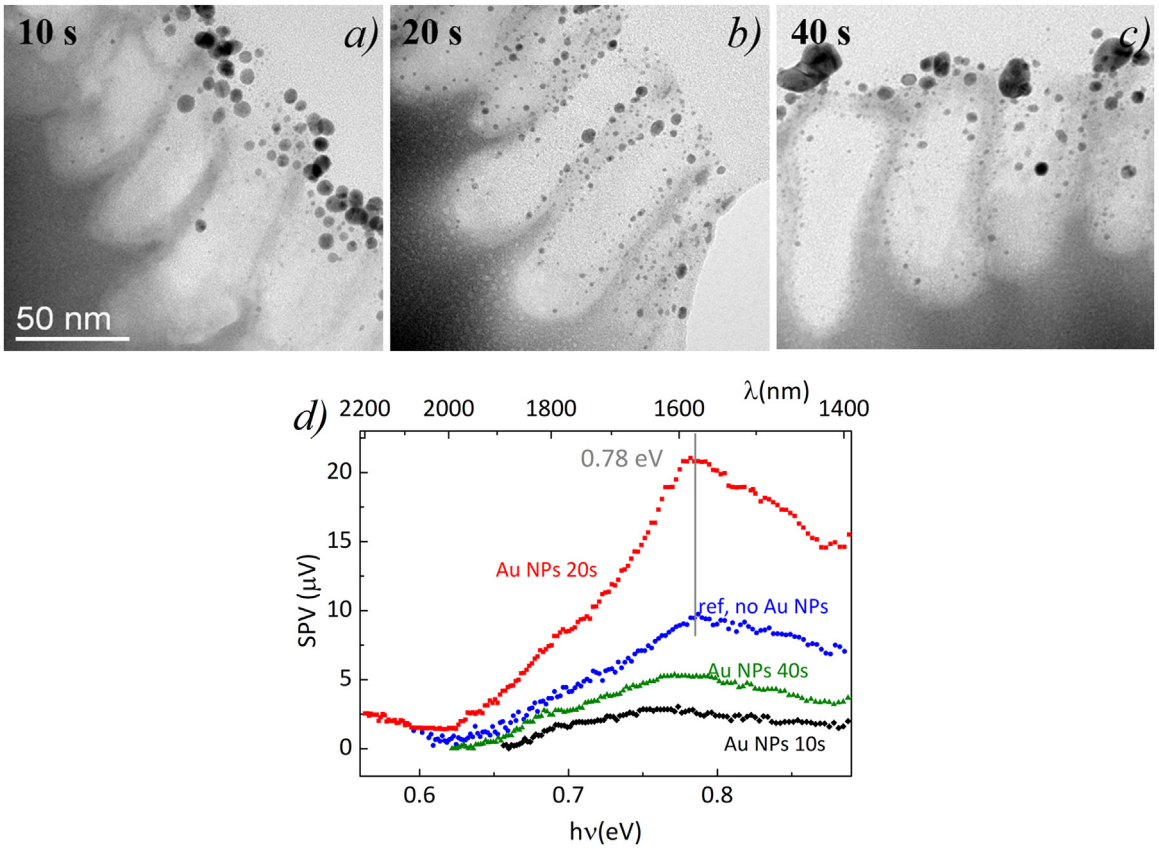

Fig. 8. X-TEM micrograph pictures of Au nanoparticles embedded within the np-Ge structure deposited with a) 10 s, b) 20 s and c) 40 s, respectively. d) SPV signal versus photon energy for np-Ge samples decorated with gold nanoparticles for different deposition times, compared with non-decorated sample. Fluence: 1×10^{16} cm^{-2}, as deposited. *Reprinted from* [44].

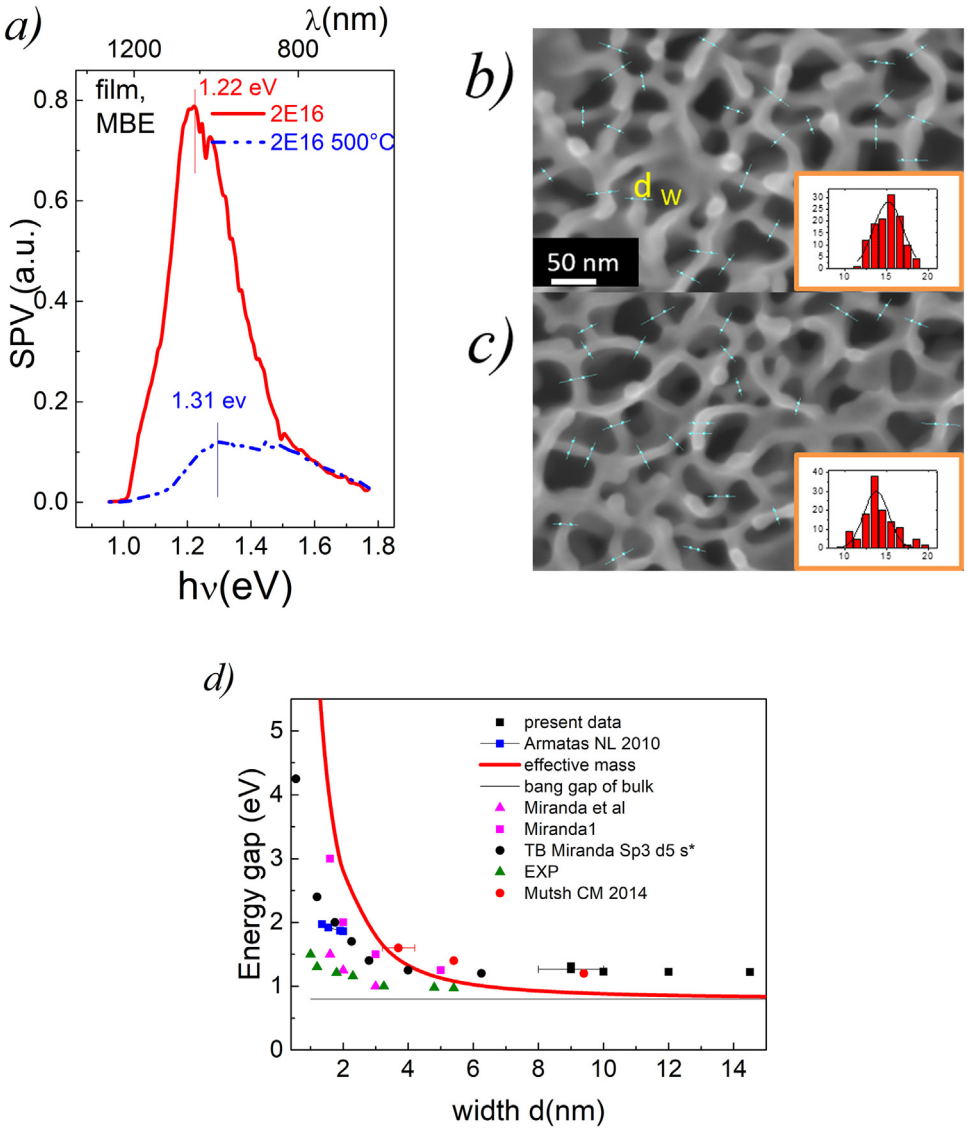

Fig. 9. a) Surface photovoltage spectra of film MBE np-Ge layers implanted at 2E16 Ge^{+}/cm^{-2} before and after a 500 °C annealing step. SEM plan view of b) as implanted and c) annealed samples. Examples of data lines used for statistical wall size sampling are reported in light blue. A scale marker of 50 nm is the same for both images, and inset histogram abscissa has unit of nm. d) Measured energy gap values (black square dots with error bars) plotted as a function of the average wall size d compared with experimental literature data [53,54,560,61], theoretical literature data [55] and effective mass model (solid red line). *Reprinted from* [45]. (For interpretation of the references to color in this figure legend, the reader is referred to the web version of this article.).

times. The X-TEM pictures (Fig. 8a–c) reveal the explanation of this behaviour: it is evident that only in the case of 20 s deposition time small diameters Au NPs (1–5 nm range) coat the inner walls of the porous structure (Fig. 8b), while 10 and 40 s deposition times produce large Au nanoparticles (diameters > 20 nm), which mainly remain located at the top of the columns (Fig. 8a,c). In other words, the presence of large Au NPs at the top of the columns could lead to photovoltage suppression, while deeper located small NPs are effective in its enhancement. This effect can be explained as follows: the location of large NP clusters at the top surface leads to an enhanced surface recombination; the surface band bending reduces as well as its variation with impinging photons, i.e. the SPV signal. In contrast, small nanoparticles located in the nanopore interior act as effective scattering centres for light. They possibly promote the bouncing of the incoming photon within the nanopore, driving an effective light trapping process. Moreover, the photovoltage enhancement mostly takes place at around 1650 nm, at wavelengths very close to the Ge band-to-band transitions. On the contrary, this spectral region is far from the energy range of Au NPs surface plasmon resonance [51]. Therefore, the surface plasmonic resonance effects on the observed SPV signal enhancement can be ruled out, leaving the light scattering from the metallic nanoparticles as its only cause.

This last example shows the potentiality of SPV spectroscopy to reveal phase changes and light trapping phenomena.

Np-Ge thin films have also been investigated by SPV method and their spectra are reported in Fig. 9a. np-Ge thin films implanted with a fluence of 2×10^{16} Ge^{+}/cm^{-2} before and after annealing treatment at 500 °C are compared. The illumination condition has been kept the same for both measurements. The annealing step leads to a significant blue shift of the energy gap, from 1.22 to 1.31 eV, as well as to a strong attenuation of the signal intensity. The strong suppression of the SPV signal intensity after annealing has been also observed for the samples with different implant fluence (1×10^{16} Ge^{+}/cm^{-2}). The decrease of the signal can be related to the observed Si-Ge intermixing at the interface (see [52] for details): a diffusion of Si from the SiO_2 substrate allows for the formation of a Si-Ge phase at the interface. This phase has been observed in literature at annealing temperatures close to 500 °C [53]. The formation of a chaotic interface between Ge and SiO_2 promotes recombination processes, reducing the SPV signal. As regards the blue shift in Fig. 9a, it has already been observed in sputter deposited thin film np-Ge samples [45]. Scanning Electron Microscopy (SEM) analyses of the two samples (Fig. 9b,c) clarify this effect due to annealing (Fig. 9a). The porous structure clearly consists of pores separated by walls of dimensions in the nm range. A careful analysis on several micrographs at different magnification of the wall size (d_W) resulted in the distributions plotted in the insets of Fig. 9b,c. A change

in the d_W distribution range due to annealing has been measured, from 12 to 17 nm for the np-Ge as-implanted sample, to 9–15 nm for the annealed one. The observed blue shift can be explained by the average wall size decrease upon annealing, considering a quantum confinement mechanism of free electrons inside the walls. This assumption is in accordance with the work of Armatas et al. [54]. Moreover, a broadening of the d_W distribution, as well as of the SPV peak, occur after annealing.

To better understand the observed blue shift effect in nanoporous Ge films, measured energy gap values have been plotted as a function of the average wall sizes d_W of the samples obtained by scanning electron micrograph (Fig. 9d) and compared with published experimental results obtained for nanoporous Ge [54] and Ge nanocrystals [10]. Theoretical and experimental results replotted from [55] as a function of the confinement dimension d are also added to Fig. 9d. The dependence of the energy gap on d is also calculated by the effective mass model formula and plotted in Fig. 9d as a red solid line. A quite large dispersion among the results is evident due to several reasons. Firstly, the effective mass theory is an approximated model; secondly, experimental data here plotted are measured by different spectroscopy methods (emission and absorption) and, in addition, they refer to various nanostructures (ordered nanoporous structures, nanocrystals and nanowires) embedded in different matrices. Moreover, beside the different embedding medium [56], also the surface termination should affect the results. In the present case, the existence of a Ge-O termination layer at the surface of our structures has been assumed [57]. Nevertheless, it is interesting to note in Fig. 9d how our experimental data (black squares) agree with the results obtained by Muthuswamy et al. [10] on Ge nanocrystals by SPV (red dots).

A clear blue-shift of the energy gap with decreasing d_w has already been observed by SPV spectroscopy. It occurred in colloidal nanocrystals [58] and consistently large Ge Bohr radius [59], for confinement dimensions up to 14 nm. Nevertheless, a similar effect has never been observed in bulk np-Ge samples. A possible explanation is reported in [45]: in bulk np-Ge samples, the photo-generated free carriers could lose confinement since nothing prevent their motion from the nanoporous layer to the continuously connected Ge substrate. On the contrary, in np-Ge thin layers, a potential barrier at the interface with SiO_2 force the carriers to be confined within the nanostructure, avoiding them to reach the substrate.

4. Conclusions

The aim of this review is to present the application of the Surface Photovoltage Spectroscopy method to different semiconductor low dimensional structures important for applications in the optical field.

SPV spectroscopy has allowed to characterize buried layers in III-N based heterostructures, where the effect that the 2-dimensional electron gas forming in InAlGaN/GaN has on the energy gap value has been demonstrated. Impurity related levels, gap values and bowing parameters have been obtained in InGaN/GaN heterojunctions as a function of In content.

The detection of electronic transitions in Si nanowires helped us obtaining evidence of doping-induced phase changes in Si nanowires. Quantum confinement effects have been demonstrated in Si nanocrystals in two different systems: nc-Si:H and nc-SiO_xN_y films.

Finally, the application of the method to nanoporous Ge has contributed to the identification of phase transitions induced by thermal treatment, enhanced light trapping effects due to Au nanoparticles embedded in the np-Ge matrix and quantum confinement effects in nanoporous Ge films.

In conclusion, the reported examples evidence the potential, the flexibility and the ease of application of the Surface Photovoltage method, that can be used to investigate a wide range of different systems allowing to achieve important physical information on material properties that can hardly be otherwise obtained.

Acknowledgments

Beatrice Fraboni and Anna Cavallini from University of Bologna, Italy, Albert Minj and Pierre Rutherana from ENSI-CAEN, France, Saurabh Pandey from Nexperia Manchester, U.K, Giancarlo Salviati from IMEM-CNR Parma, Italy, Lucia Romano from Paul Scherrer Institute, Switzerland, Giuliana Impellizzeri from IMM-CNR Catania, Italy, Maria Grazia Grimaldi from University of Catania, Italy, Barbara Terheiden from University of Konstanz, Germany, are all acknowledged for providing samples and useful discussions; Filippo Maria Giorgi and Bruna Dudda from University of Bologna, Italy, for technical assistance and SPV measurements.

References

[1] H.C. Gatos, J. Lagowski, Surface photovoltage spectroscopy - A new approach to the study of high-gap semiconductor surfaces, J. Vac. Sci. Technol. 10 (1973) 130–135, http://dx.doi.org/10.1116/1.1317922.
[2] D.K. Schroder, Surface voltage and surface photovoltage: history, theory and applications, Meas. Sci. Technol. 12 (2001) R16–R31, http://dx.doi.org/10.1088/0957-0233/12/3/202.
[3] L. Kronik, Y. Shapira, Surface photovoltage phenomena: theory, experiment, and applications, Surf. Sci. Rep. 37 (1999) 1–206, http://dx.doi.org/10.1016/S0167-5729(99)00002-3.
[4] L. Kronik, Y. Shapira, Surface photovoltage spectroscopy of semiconductor structures: at the crossroads of physics, chemistry and electrical engineering, Surf. Interface Anal. 31 (2001) 954–965, http://dx.doi.org/10.1002/sia.1132.
[5] J. Zhao, B.A. Nail, M.A. Holmes, F.E. Osterloh, Use of surface photovoltage spectroscopy to measure built-in voltage, space charge layer width, and effective band gap in CdSe quantum dot films, J. Phys. Chem. Lett. 7 (2016) 3335–3340, http://dx.doi.org/10.1021/acs.jpclett.6b01569.
[6] M.J. Shearer, M.-Y. Li, L.-J. Li, S. Jin, R.J. Hamers, Nanoscale surface photovoltage mapping of 2D materials and heterostructures by illuminated Kelvin probe force microscopy, J. Phys. Chem. C. (2018), http://dx.doi.org/10.1021/acs.jpcc.7b12579.
[7] M.A. Melo, Z. Wu, B.A. Nail, A.T. De Denko, A.F. Nogueira, F.E. Osterloh, Surface photovoltage measurements on a particle tandem photocatalyst for overall water splitting, Nano Lett. 18 (2018) 805–810, http://dx.doi.org/10.1021/acs.nanolett.7b04020.
[8] T. Dittrich, C. Awino, P. Prajongtat, B. Rech, M.C. Lux-Steiner, Temperature dependence of the band gap of $CH_3NH_3PbI_3$ stabilized with PMMA: a modulated surface photovoltage study, J. Phys. Chem. C. 119 (2015) 23968–23972, http://dx.doi.org/10.1021/acs.jpcc.5b07132.
[9] L. Barnea-Nehoshtan, S. Kirmayer, E. Edri, G. Hodes, D. Cahen, Surface photovoltage spectroscopy study of organo-lead perovskite solar cells, J. Phys. Chem. Lett. 5 (2014) 2408–2413, http://dx.doi.org/10.1021/jz501163r.
[10] E. Muthuswamy, J. Zhao, K. Tabatabaei, M.M. Amador, M.A. Holmes, F.E. Osterloh, S.M. Kauzlarich, Thiol-capped germanium nanocrystals: preparation and evidence for quantum size effects, Chem. Mater. 26 (2014) 2138–2146, http://dx.doi.org/10.1021/cm4042154.
[11] E. Kim, Y. Cho, A. Sohn, H. Hwang, Y.U. Lee, K. Kim, H.-H. Park, J. Kim, J.W. Wu, D.-W. Kim, Mie resonance-modulated spatial distributions of photogenerated carriers in poly(3-hexylthiophene-2,5-diyl)/silicon nanopillars, Sci. Rep. 6 (2016) 29472, http://dx.doi.org/10.1038/srep29472.
[12] T. Yao, R. Chen, J. Li, J. Han, W. Qin, H. Wang, J. Shi, F. Fan, C. Li, Manipulating the interfacial energetics of n-type silicon photoanode for efficient water oxidation, J. Am. Chem. Soc. 138 (2016) 13664–13672, http://dx.doi.org/10.1021/jacs.6b07188.
[13] D. Jana, T.K. Sharma, A correlation between the defect states and yellow luminescence in AlGaN/GaN heterostructures, J. Appl. Phys. 122 (2017) 035101, http://dx.doi.org/10.1063/1.4993903.
[14] D. Cavalcoli, B. Fraboni, A. Cavallini, Chapter seven - Surface and defect states in semiconductors investigated by surface photovoltage, Defects Semicond. 91 (2015) 251–278, http://dx.doi.org/10.1016/bs.semsem.2014.11.004.
[15] J. Wu, When group-III nitrides go infrared: new properties and perspectives, J. Appl. Phys. 106 (2009) 011101, http://dx.doi.org/10.1063/1.3155798.
[16] S.-H. Lim, Y.-H. Ko, C. Rodriguez, S.-H. Gong, Y.-H. Cho, Electrically driven, phosphor-free, white light-emitting diodes using gallium nitride-based double concentric truncated pyramid structures, Light Sci. Appl. 5 (2016) e16030, http://dx.doi.org/10.1038/lsa.2016.30.
[17] A. Minj, H. Ben Ammar, A. Cros, N. Garro, P. Gamarra, S.L. Delage, P. Ruterana, Probing the local electrical properties of Al(In,Ga)N by Kelvin probe force microscopy, Phys. Status Solidi 255 (2018) 1700427, http://dx.doi.org/10.1002/pssb.201700427.
[18] S. Pandey, D. Cavalcoli, A. Cavallini, Band bowing and Si donor levels in InGaN layers investigated by surface photo voltage spectroscopy, Appl. Phys. Lett. 102 (2013) 142101, http://dx.doi.org/10.1063/1.4799658.
[19] P.G. Moses, C.G. Van de Walle, Band bowing and band alignment in InGaN alloys, Appl. Phys. Lett. 96 (2010) 021908, http://dx.doi.org/10.1063/1.3291055.
[20] J. Wu, W. Walukiewicz, K.M. Yu, J.W. Ager, E.E. Haller, H. Lu, W.J. Schaff, Small band gap bowing in $In_{1-x}Ga_xN$ alloys, Appl. Phys. Lett. 80 (2002) 4741–4743,

http://dx.doi.org/10.1063/1.1489481.
[21] J. Wu, W. Walukiewicz, W. Shan, K.M. Yu, J.W. Ager, S.X. Li, E.E. Haller, H. Lu, W.J. Schaff, Temperature dependence of the fundamental band gap of InN, J. Appl. Phys. 94 (2003) 4457–4460, http://dx.doi.org/10.1063/1.1605815.
[22] I. Gorczyca, T. Suski, N.E. Christensen, A. Svane, Size effects in band gap bowing in nitride semiconducting alloys, Phys. Rev. B. 83 (2011) 153301, http://dx.doi.org/10.1103/PhysRevB.83.153301.
[23] C.J. Neufeld, S.C. Cruz, R.M. Farrell, M. Iza, J.R. Lang, S. Keller, S. Nakamura, S.P. DenBaars, J.S. Speck, U.K. Mishra, Effect of doping and polarization on carrier collection in InGaN quantum well solar cells, Appl. Phys. Lett. 98 (2011) 243507, http://dx.doi.org/10.1063/1.3595487.
[24] M.T. Hardy, E.C. Young, P. Shan Hsu, D.A. Haeger, I.L. Koslow, S. Nakamura, S.P. DenBaars, J.S. Speck, Suppression of *m*-plane and *c*-plane slip through Si and Mg doping in partially relaxed (202¯1) InGaN/GaN heterostructures, Appl. Phys. Lett. 101 (2012) 132102, http://dx.doi.org/10.1063/1.4754693.
[25] M. Gonschorek, J.-F. Carlin, E. Feltin, M.A. Py, N. Grandjean, V. Darakchieva, B. Monemar, M. Lorenz, G. Ramm, Two-dimensional electron gas density in $Al_{1-x}In_xN$/AlN/GaN heterostructures ($0.03 \le x \le 0.23$), J. Appl. Phys. 103 (2008) 093714, http://dx.doi.org/10.1063/1.2917290.
[26] S. Pandey, B. Fraboni, D. Cavalcoli, A. Minj, A. Cavallini, Two-dimensional electron gas properties by current-voltage analyses of $Al_{0.86}$ $In_{0.14}N$/AlN/GaN heterostructures, Appl. Phys. Lett. 99 (2011) 012111, http://dx.doi.org/10.1063/1.3608162.
[27] D. Cavalcoli, S. Pandey, B. Fraboni, A. Cavallini, Band gap shift in $Al_{1-x}In_xN$/AlN/GaN heterostructures studied by surface photovoltage spectroscopy, Appl. Phys. Lett. 98 (2011) 142111, http://dx.doi.org/10.1063/1.3576938.
[28] NSM Archive - Gallium Nitride (GaN) - Band structure (n.d.). 〈http://www.ioffe.ru/SVA/NSM/Semicond/GaN/bandstr.html〉 (Accessed 28 February 2018).
[29] F. Priolo, T. Gregorkiewicz, M. Galli, T.F. Krauss, Silicon nanostructures for photonics and photovoltaics, Nat. Nanotechnol. 9 (2014) 19–32, http://dx.doi.org/10.1038/nnano.2013.271.
[30] M.M. Adachi, M.P. Anantram, K.S. Karim, Optical properties of crystalline – amorphous core – shell silicon nanowires, Nano Lett. 10 (2010) 4093–4098, http://dx.doi.org/10.1021/nl102183x.
[31] Y. Qu, L. Liao, Y. Li, H. Zhang, Y. Huang, X. Duan, Electrically conductive and optically active porous silicon nanowires, Nano Lett. 9 (2009) 4539–4543, http://dx.doi.org/10.1021/nl903030h.
[32] F. Fabbri, E. Rotunno, L. Lazzarini, D. Cavalcoli, A. Castaldini, N. Fukata, K. Sato, G. Salviati, A. Cavallini, Preparing the way for doping wurtzite silicon nanowires while retaining the phase, Nano Lett. 13 (2013) 5900–5906, http://dx.doi.org/10.1021/nl4028445.
[33] W.C. Dash, R. Newman, Intrinsic optical absorption in single-crystal germanium and silicon at 77 K and 300 K, Phys. Rev. 99 (1955) 1151–1155, http://dx.doi.org/10.1103/PhysRev.99.1151.
[34] D. Cavalcoli, M. Rossi, A. Cavallini, Defect states in nc-Si:H films investigated by surface photovoltage spectroscopy, J. Appl. Phys. 109 (2011) 053719, http://dx.doi.org/10.1063/1.3553583.
[35] L. Bagolini, A. Mattoni, L. Colombo, Electronic localization and optical absorption in embedded silicon nanograins, Appl. Phys. Lett. 94 (2009) 053115, http://dx.doi.org/10.1063/1.3078281.
[36] N. Brinkmann, D. Sommer, G. Micard, G. Hahn, B. Terheiden, Electrical, optical and structural investigation of plasma-enhanced chemical-vapor-deposited amorphous silicon oxynitride films for solar cell applications, Sol. Energy Mater. Sol. Cells 108 (2013) 180–188, http://dx.doi.org/10.1016/j.solmat.2012.09.025.
[37] M. Perani, N. Brinkmann, A. Hammud, D. Cavalcoli, B. Terheiden, Nanocrystal formation in silicon oxy-nitride films for photovoltaic applications: optical and electrical properties, J. Phys. Chem. C. 119 (2015) 13907–13914, http://dx.doi.org/10.1021/acs.jpcc.5b02286.
[38] J. Seiffe, L. Gautero, M. Hofmann, J. Rentsch, R. Preu, S. Weber, R.A. Eichel, Surface passivation of crystalline silicon by plasma-enhanced chemical vapor deposition double layers of silicon-rich silicon oxynitride and silicon nitride, J. Appl. Phys. 109 (2011) 034105, http://dx.doi.org/10.1063/1.3544421.
[39] R. Koole, E. Groeneveld, D. Vanmaekelbergh, A. Meijerink, C. de Mello Donegá, Size effects on semiconductor nanoparticles, Nanoparticles, Springer Berlin Heidelberg, Berlin, Heidelberg, 2014, pp. 13–51, , http://dx.doi.org/10.1007/978-3-662-44823-6_2.
[40] I. Sychugov, F. Pevere, J.-W. Luo, A. Zunger, J. Linnros, Single-dot absorption spectroscopy and theory of silicon nanocrystals, Phys. Rev. B. 93 (2016) 161413, http://dx.doi.org/10.1103/PhysRevB.93.161413.
[41] H. Föll, J. Carstensen, S. Frey, Porous and nanoporous semiconductors and emerging applications, J. Nanomater. 2006 (2006) 1–10, http://dx.doi.org/10.1155/JNM/2006/91635.
[42] T. Dittrich, I. Mora-Seró, G. García-Belmonte, J. Bisquert, Temperature dependent normal and anomalous electron diffusion in porous TiO_2 studied by transient surface photovoltage, Phys. Rev. B. 73 (2006) 045407, http://dx.doi.org/10.1103/PhysRevB.73.045407.
[43] L. Burstein, Y. Shapira, J. Partee, J. Shinar, Y. Lubianiker, I. Balberg, Surface photovoltage spectroscopy of porous silicon, Phys. Rev. B. 55 (1997) R1930–R1933, http://dx.doi.org/10.1103/PhysRevB.55.R1930.
[44] D. Cavalcoli, B. Fraboni, G. Impellizzeri, L. Romano, E. Scavetta, M.G. Grimaldi, Optoelectronic properties of nanoporous Ge layers investigated by surface photovoltage spectroscopy, Microporous Mesoporous Mater. 196 (2014) 175–178, http://dx.doi.org/10.1016/J.MICROMESO.2014.05.013.
[45] D. Cavalcoli, G. Impellizzeri, L. Romano, M. Miritello, M.G. Grimaldi, B. Fraboni, Optical properties of nanoporous germanium thin films, ACS Appl. Mater. Interfaces 7 (2015) 16992–16998, http://dx.doi.org/10.1021/acsami.5b02089.
[46] X.T. Wang, W.S. Shi, G.W. She, L.X. Mu, S.T. Lee, High-performance surface-enhanced Raman scattering sensors based on Ag nanoparticles-coated Si nanowire arrays for quantitative detection of pesticides, Appl. Phys. Lett. 96 (2010) 053104, http://dx.doi.org/10.1063/1.3300837.
[47] K. Saha, S.S. Agasti, C. Kim, X. Li, V.M. Rotello, Gold nanoparticles in chemical and biological sensing, Chem. Rev. 112 (2012) 2739–2779, http://dx.doi.org/10.1021/cr2001178.
[48] L. Romano, G. Impellizzeri, M.V. Tomasello, F. Giannazzo, C. Spinella, M.G. Grimaldi, Nanostructuring in Ge by self-ion implantation, J. Appl. Phys. 107 (2010) 084314, http://dx.doi.org/10.1063/1.3372757.
[49] G. Impellizzeri, L. Romano, B. Fraboni, E. Scavetta, F. Ruffino, C. Bongiorno, V. Privitera, M.G. Grimaldi, Nanoporous Ge electrode as a template for nano-sized (< 5 nm) Au aggregates, Nanotechnology 23 (2012) 395604, http://dx.doi.org/10.1088/0957-4484/23/39/395604.
[50] G. Impellizzeri, L. Romano, L. Bosco, C. Spinella, M.G. Grimaldi, Nanoporosity induced by ion implantation in germanium thin films grown by molecular beam epitaxy, Appl. Phys. Express 5 (2012) 035201, http://dx.doi.org/10.1143/APEX.5.035201.
[51] S. Eustis, M.A. El-Sayed, Why gold nanoparticles are more precious than pretty gold: noble metal surface plasmon resonance and its enhancement of the radiative and nonradiative properties of nanocrystals of different shapes, Chem. Soc. Rev. 35 (2006) 209–217, http://dx.doi.org/10.1039/B514191E.
[52] L. Romano, G. Impellizzeri, M.G. Grimaldi, Influence of microstructure on voids nucleation in nanoporous Ge, Mater. Lett. 96 (2013) 74–77, http://dx.doi.org/10.1016/J.MATLET.2013.01.017.
[53] L. Ding, A.E.-J. Lim, J.T.-Y. Liow, M.B. Yu, G.-Q. Lo, Dependences of photoluminescence from P-implanted epitaxial Ge, Opt. Express 20 (2012) 8228, http://dx.doi.org/10.1364/OE.20.008228.
[54] G.S. Armatas, M.G. Kanatzidis, Size dependence in hexagonal mesoporous germanium: pore wall thickness versus energy gap and photoluminescence, Nano Lett. 10 (2010) 3330–3336, http://dx.doi.org/10.1021/nl101004q.
[55] S. Parola, E. Quesnel, V. Muffato, J. Bartringer, A. Slaoui, Influence of the embedding matrix on optical properties of Ge nanocrystals-based nanocomposite, J. Appl. Phys. 113 (2013) 053512, http://dx.doi.org/10.1063/1.4789959.
[56] S.K. Ray, S. Maikap, W. Banerjee, S. Das, Nanocrystals for silicon-based light-emitting and memory devices, J. Phys. D. Appl. Phys. 46 (2013) 153001, http://dx.doi.org/10.1088/0022-3727/46/15/153001.
[57] Z.C. Holman, U.R. Kortshagen, Absolute absorption cross sections of ligand-free colloidal germanium nanocrystals, Appl. Phys. Lett. 100 (2012) 133108, http://dx.doi.org/10.1063/1.3698091.
[58] A. Miranda, A. Trejo, E. Canadell, R. Rurali, M. Cruz-Irisson, Interconnection effects on the electronic and optical properties of Ge nanostructures: a semi-empirical approach, Phys. E Low.-Dimens. Syst. Nanostruct. 44 (2012) 1230–1235, http://dx.doi.org/10.1016/J.PHYSE.2012.01.017.
[59] Y. Maeda, N. Tsukamoto, Y. Yazawa, Y. Kanemitsu, Y. Masumoto, Visible photoluminescence of Ge microcrystals embedded in SiO_2 glassy matrices, Appl. Phys. Lett. 59 (1991) 3168–3170, http://dx.doi.org/10.1063/1.105773.
[60] L.M. Wheeler, L.M. Levij, U.R. Kortshagen, Tunable band gap emission and surface passivation of germanium nanocrystals synthesized in the gas phase, J. Phys. Chem. Lett. 4 (2013) 3392–3396, http://dx.doi.org/10.1021/jz401576b.
[61] R.K. Singha, S. Manna, S. Das, A. Dhar, S.K. Ray, Room temperature infrared photoresponse of self assembled Ge/Si (001) quantum dots grown by molecular beam epitaxy, Appl. Phys. Lett. 96 (2010) 233113, http://dx.doi.org/10.1063/1.3446848.